Hall Thrusters Operating in Pulsed Mode

Vlad Hruby, Bruce Pote, Manuel Gamero-Castaño, George Kolencik,
Larry Byrne, Rachel Tedrake and Mary Delichatsios
Busek Co. Inc.
11 Tech Circle
Natick, MA 01760-1023
busek@busek.com
508-655-5565

IEPC-01-66

Heretofore, Hall thrusters were perceived as strictly steady state devices, unsuitable for operation in a pulsed mode. We have demonstrated that at least certain types of Hall thrusters can efficiently deliver thrust pulses with a duration as short as few tens of msec.

Our 200 W Hall thruster, designated BHT-200, was pulsed nearly 500,000 times delivering precisely controllable, repetitive impulse bits of arbitrary magnitude starting as low as sub mNsec. This was achieved without significant loss of efficiency and a moderate loss of specific impulse due to xenon flow timing. The thruster was driven by both a PPU and by discharging a capacitor in the so called direct drive pioneered by others. This demonstration opens a new field of applicability for the tandem style and possibly other Hall thrusters that was previously reserved to PPTs and cold gas thrusters. This includes attitude control and primary propulsion for microspacecraft that lack sufficient power for continuous operation at 200 W. For spacecraft with sufficient power on board, the same Hall thruster can be used for both primary and ACS propulsion.

The paper treats the subject in a generic manner describing the various methods of pulsed mode operation, flow and electrical start-up transients, system requirements and areas of applicability. This description is supported by analytical models and data from the pulsed BHT-200 experiments.

1.0 Introduction and Pulsed Hall Thruster Applications

Heretofore, Hall thrusters were perceived as devices suitable only for steady state operation. As will be described in this paper we have demonstrated that at least some types of Hall thrusters can be pulsed with a pulse duration as short as few tens of msec and deliver nearly steady state performance. Busek's 200 W tandem style Hall thruster demonstrated that it can efficiently produce impulses ranging from a mNsec to nearly infinity, limited only by its lifetime.

Presented as Paper IEPC-01-66 at the 27th International Electric Propulsion Conference, Pasadena, CA, 15-19 October 2001

For the variable impulse it can be powered by a conventional PPU, capacitor discharge thus eliminating conventional PPU, and in some configurations directly from solar panels. With advanced capacitors the necessary energy can be stored in 1-in cube. With these capabilities and lower complexity/cost of some configurations, a whole new range of applications emerges that includes propulsion for power limited micro or nano spacecraft, ACS (attitude control system) propulsion for large spacecraft that already have Xe on board and general, combined steady state and pulsed thrusting using the same Hall thruster on a wide variety of spacecraft. These applications are briefly discussed below.

1.1 Microspacecraft Propulsion

High ΔV, microsatellite missions require high Isp propulsion. This can be provided only by electric thrusters such as PPT's, FEEP's, and colloid thrusters and perhaps by continuously operating, very low power, Xe fed, ion and Hall thrusters. Small ion and Hall thrusters (<100 W) have poor performance and probably are too large for the available power on a typical microspacecraft. PPT's are inefficient (~10%) and tend to overheat when operated above some tens of watts. FEEPs and colloids are not suitable for a mN or larger thrust.

The pulsed Hall thruster system for nano or microspacecraft could be powered from a capacitor, substantially smaller than that used in current PPT's, eliminating the most expensive part of the conventional system, which is the PPU discharge converter.

Reconfiguring a group of capacitors from a paralled connection for charging to seriesed connection for discharging allows the system to operate directly from a low voltage photo voltaic array – the so called direct drive studied by others[1,2]. Depending on the pulse duration and the rep. rate, efficient operation can be achieved down to few Watts average power consumption.

1.2 ACS for Large Xe Fueled Spacecraft

Gridded ion thrusters and Hall thrusters using Xe propellant, are the propulsion of choice for large S/C with missions requiring significant ΔV. This includes station keeping, orbit repositioning, orbit raising and deep space missions such as the DS1[3]. However, as mentioned above, they are not suitable for low ΔV, ACS function and for very small power limited satellites. This is due to two reasons: (1) ACS usually requires accurate impulse bits which are difficult to produce by the conventional ion and Hall thrusters; and (2) plasma thrusters of all types are difficult to scale down below about 100 W without very significant performance penalty. The low ΔV, ACS functions therefore continue to be performed by cold gas thrusters, hydrazine monoprops, resistojets and most recently by Teflon fueled PPT's. The spacecraft must then carry the large Xe fueled, ion or Hall thrusters and the ACS thrusters fueled by other propellants with the concomitant complication with dual tankage, controls, etc.

The lack of fuel commonality increases the S/C cost and complexity which prompted NASA to initiate development of Xe resistojet.[4] While resistojets can deliver impressive thrust at low input power, their Isp with Xe is typically less than 100 sec, an order of magnitude below that of even very small Hall thrusters. Additionally they are difficult to operate in a pulsed mode for delivery of well defined impulse bits unless they operate as a cold gas thruster which further reduces their Isp. For some missions this may be significant enough to impact the benefits of the conventional, station keeping Hall or ion propulsion on board of the S/C.

The perception in the community, however, is that ACS propulsion using Xe is not needed because of the simplicity of PPTs. That simplicity, however, comes at the cost of very low efficiency (~10%) and significant potential for S/C contamination by Teflon particles[5]. It therefore appears, that both the Xe resistojet and the Teflon PPT have some undesirable features that Xe fueled ACS propulsion with high Isp and high efficiency would avoid.

1.3 Combined Continuous and Pulsed Primary Propulsion

Many missions especially those involving multiple satellites in coordinated formation flight, require high Isp, high efficiency, primary propulsion for the final orbit acquisition (after drop off from the launch vehicle), on-orbit repositioning and orbit maneuvering to reconfigure the formation. An example of such a mission is TechSat 21[6] with a ΔV≥60 m/sec while also requiring a minimum impulse bit of 2 mNsec for close proximity maneuvering. Prior to the pulsed Hall thruster, the TS21 mission would have required drastically different modes of propulsive operation which up to now required different types of thrusters for each segment of the mission.

We have shown that our tandem style Hall thrusters can fulfill the requirements of all segments of the TS21 mission which was the original motivator for more systematic pulsed thruster investigations. For the orbit acquisition the Hall thruster operate in a continuous, steady state firing mode lasting many minutes. For the formation reconfiguration or ACS functions the same Hall thruster can operate in short pulses to deliver precise impulse bits to the spacecraft.

1.4 Microsat Mission Example

Consider the recent NASA New Millennium solicitation for the ST5 Small Satellites Technology demonstration which specified the following mission requirements:

1. A spacecraft with a mass of 20 kg, capable of delivering 20 Watts of power to all loads. (We assumed that 10 W can be taken for propulsion.)
2. The propulsion is required to provide the following ΔV's
   - orbit initialization ΔV =350m/sec
   - orbit maintenance ΔV = 100 m/sec
   - ACS, one full 360° rotation of S/C in total
3. Maximum propulsion system dry and wett mass of l.5 kg and 5 kg respectively.

We now examine if these requirements could be met with one pulsed BHT-200 using a simple capacitive drive shown in Figure 1. Energy conservation requires that 10W $\tau_{charge} \geq$ 200 W τ_{dis}

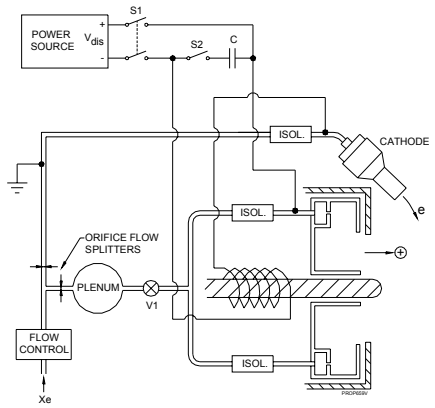

Figure 1 Schematic of the flow and power system for pulsed BHT-200

Selecting τ_{dis} = 10msec, yields τ_{charge} = 200 msec ≈ τ_{period}. This yields 5Hz rep rate. Total ΔV_t from above is approximately 450 m/sec (ignoring ACS) and therefore momentum conservation requires the total operating time to be $\tau_{op} \cong {}^{m_{s/c}\Delta V_t}\!/_{T}$. The 200 W thruster delivers T=11 mN which yields $\tau_{op} \cong 8.18 \times 10^5$ sec (=227 hours of total operating time) and the number of pulses $N=\tau_{op}/\tau_{dis} \cong 8.18 \times 10^7$ cycles. This may be a border line of the capability of fast acting valves which is a drawback of this concept, to be countered by extending τ_{dis} and/or putting two valves in series. The total elapsed time to execute the orbit initialization with ΔV = 350 m/sec is $\tau_{oi}=\tau_{op}\tau_{period}/\tau_{dis} \cong 1.27 \times 10^7$ sec = l47 days. If we assume that all 20 W could be used for propulsion, the orbit initialization would be about 74 days and the number of cycles would be also cut in half.

Assuming average I_{sp} of 1200 we get the total required propellant mass M_p = 0.75 kg and a total estimated system weight of about 4 kg. We assumed I_{sp} = 1200 sec instead of the demonstrated 1570 sec to account for losses during the transients when a fast acting valve opens filling the discharge cavity. The dynamics of the propellant supply is an important issue which will be discussed later.

The capacitor discharge energy is E= (200 W) (10 msec) = 2 Joules. Assuming starting and pulse ending applied voltage of 300 and 290 volts respectively, yields capacitance C = 0.68 mF. If we select an advanced MF type capacitor,[7] its mass

would be 2J/95mJ/gram = 21 grams and its volume would be 2J/150mJ/cc = 13.3 cm^3 ≅1" x 1"x 1" cube. Whether such a small volume can provide almost 0.7 mF will have to be investigated, but it is clear that the estimated volume and weight including the 10 W charger is substantially below a 200 W PPU that is estimated to weigh 3 to 4 kg. As stated above, the total estimated pulsed Hall thruster system weight is 4.0 kg and higher required ΔV would be more favorable relative to cold gas, chemical or PPT alternatives.

2.0 Pulsing Methods

A simplified pulsed Hall thruster system schematic is shown in Figure 1. It represents one of several possible arrangements using as an example Busek's 200 Watt tandem style thruster[8] with a single electromagnetic coil. There are three fundamental ways to pulse the thruster.

1. Flow Pulsing – Turn on and off a fast acting valve V_1 located immediately upstream of the thruster to minimize volume between it and the discharge chamber. Assuming that the cathode is ready to deliver electrons and that the anode is at a sufficient potential (V_d) the discharge will start when sufficient pressure builds up inside the discharge cavity following V_1 opening. Because in Figure 1 the discharge is in series with the magnet coil, the required radial magnetic field will build up simultaneously with discharge current flowing through the closed S1 or S2 switches. When V_1, closes the discharge cavity pressure decreases and the discharge turns off.
2. Power Pulsing – Turn on the discharge power while V_1 is opened and the plasma gas is flowing. Sufficient potential at the anode will start the discharge. The pulse is terminated by opening the indicted switches.
3. Combination of Flow and Power Pulsing – This is in general a desirable approach because it minimizes propellant consumption achieved by flow pulsing while eliminating discharge transients during flow-on/off transitions.

3.0 Thruster Sizing and Performance

One of the key questions is the selection of the thruster size. Consider the following example. A spacecraft can provide 25 Watts of power to the thruster system continuously. What thruster should be developed? A 25 W thruster operating continuously, a 50 W thruster pulsed with 50% duty cycle or a 200 W thruster pulsed at 12.5% duty cycle. While a complete answer requires mission and detailed system analysis, we can estimate the DC performance of these thrusters to determine if the expected performance degradation with reduced size is severe enough to offset losses incurred by low duty cycle (i.e. short pulse length relative to starting transients) of the larger size thruster.

To answer this question we have expanded our 2 parameter analysis[9] which predicts a Hall thruster performance given input power, discharge voltage (V_{dis}), a total voltage loss (ΔV) and electron loss parameter defined as $i = I_{ee}/I_{dis}$ where I_{ee} is the cathode electron current entering the thruster and I_{dis} is the discharge current. Thus the ion beam current exiting the thruster is given $I_i = I_{dis} - I_{ee}$. In the previous work[9], both parameters ΔV and i were selected based on experimental data from similar thrusters. In the new model presented below the parameter i is predicted as a function of V_{dis}, ΔV, propellant neutral number density (n_n) and thruster dimensions which can be related to nominal thruster power and together uniquely determine the thruster Isp and efficiency (η). The approximate analytical expression for the loss parameter *i* is developed below.

The rate of ion or electron production is given by

$$\dot{n}_{ep} = n_e n_n Q_i u_e \qquad [1]$$

where n_{ep} and n_n are electron and neutral number densities respectively, Q_i is ionization cross-section and u_e is the electron velocity relative to the neutrals. Because in a Hall thruster the neutral speed is negligible and most ionization is done by the azimuthal electron flux ($J_{e\theta}$), we can replace u_e by $u_{e\theta} \cong E/B$. This approximation is valid as long as $J_{e\theta}/J_{ez} \approx \beta >> 1$ where J_{ez} is the electron axial current density and β is the Hall parameter which typically

exceeds 100 in a reasonably performing Hall thruster.

Given N_e as the total number of electrons within a discharge chamber with volume V_c, the rate at which the charge content is reduced due to flux of electrons to the walls is

$$\dot{N}_{eloss} = \frac{I_{eW}}{q} = \dot{n}_{eloss} V_c \qquad [2]$$

where I_{eW} is the current to the walls of the chamber and q is elementary charge. It follows that

$$\dot{n}_{eloss} \cong \frac{I_{eW}}{qV_c} \cong \frac{n_e u_{ew} 2\pi d_m L}{\pi d_m \Delta R L} = \frac{2n_e u_{ew}}{\Delta R} \cong \frac{2n_e}{\Delta R}\sqrt{\frac{qT_e}{m_i}} \qquad [3]$$

where ΔR is the radial width of the discharge chamber and u_{eW} is the charged particle velocity toward the wall which can be approximated by the Bohm formula for ion velocity in the presheath where $n_i \cong n_e$, and T_e is electron temperature in volts and m_i is the ion mass.

The balance between production and loss of charges results in the net rate

$$\dot{n}_{enet} = \dot{n}_{ep} - \dot{n}_{eloss} \qquad [4]$$

substituting Eqs. [1] and [3] and integrating yields

$$n_{ea} \cong n_{ee} \exp\left[\tau_n\left(\frac{1}{\tau_{ip}} - \frac{1}{\tau_{iloss}}\right)\right] \qquad [5]$$

where n_{ea} and n_{ee} are the electron number densities at the thruster anode and exit respectively. The exponent is given by three characteristic times

$$\tau_n = \frac{L_d}{\sqrt{\frac{kT_n}{m_n}}};\ \tau_{ip} = \frac{1}{n_n Q_i (E/B)};$$

$$\tau_{iloss} = \frac{1}{\frac{2}{\Delta R}\sqrt{\frac{qT_e}{m_i}}} \qquad [6]$$

where τ_n is the time for a neutral to transit the length (L_d) of the discharge chamber, τ_{ip} is the characteristic time produced an ion and τ_{iloss} is the characteristic time to loose an ion to the wall.

Using Eq. [5] and the definition of $i=I_{ee}/I_{dis}=(1-I_i/I_{dis})$ yields

$$i = 1 - \frac{u_i}{u_{ea}} \exp\left[\tau_n\left(\frac{1}{\tau_{ip}} - \frac{1}{\tau_{iloss}}\right)\right] \qquad [7]$$

]

where u_i is the ion exit velocity which from energy conservation is given by

$$u_i = \sqrt{\frac{2q}{m_i}(V_{dis} - \Delta V)} \qquad [8]$$

and u_{ea} is the electron velocity near the anode which we approximate by the Bohm cross field velocity

$$u_{ea} \approx \frac{E}{16B} \qquad [9]$$

This approximation holds in the intense discharge between the magnetic poles and is probably less accurate as both E and B drop toward the anode.

The thruster Isp and efficiency are then given by[9]

$$I_{sp} \cong \frac{u_i}{g_o};\quad \eta \cong (1-i)\left(1 - \frac{\Delta V}{V_{dis}}\right) \qquad [10]$$

Before discussing the typical results let us examine the exponential in Eq. [7]. It is clear that for a given (u_i/u_{ea}) the parameter i is minimized (i.e. efficiency is maximized) when the exponent is positive ($\tau_{ip} < \tau_{iloss}$, takes less time to create an ion than to loose it). When the exponent is negative ($\tau_{ip} > \tau_{iloss}$) the exponential is less than 1 thus increasing the parameter i and decreasing the thruster efficiency. The exponential is 1 when $\tau_{ip} = \tau_{iloss}$ when the discharge chamber radial width is

$$\Delta R = \frac{2\sqrt{\frac{qT_e}{m_i}}}{n_n Q_i \left(E/B\right)} \qquad [11]$$

for a T_e set by the discharge chamber wall material (≈ 16 eV for a BN wall) and constant *E/B* because both *E* and *B* ideally scale as 1/L or $1/\Delta R$[10]. The smaller the thruster, the larger must be the neutral density to preserve its efficiency and as long as this ideal scaling is done consistently, the thruster performance (I_{sp} and η) should be independent of thruster size.

Substituting typical values for T_e, n_n, Q_i and *E/B* into Eq. [11] yields typical ΔR in the range of 10 mm. Smaller thrusters operated at the same values of n_n and *E/B* will have lower efficiency and larger thrusters will have higher efficiency.

However, consistently scaling a thruster with B~1/L and n_n~1/L down to sizes below about 300 Watts is extremely difficult and perhaps impossible for two reasons: (1) there is no room for sufficiently large coils for the desired B and no room for iron to carry this design flux (2) the idealy scaled n_n (~1/L) results in very high power density, overheating of the thruster and short lifetime. These were the reasons why our 200 W thruster used in this study (BHT-200) departs radically from the conventional scaling and design approach. Conversely a 50 W thruster designed by Khayms[10] employing permanent and electromagnets to achieve the high B and operated high n_n rapidly overheated and achieved efficiency in single digits.

More feasible scaling is $(1/L)^n$ with n~0.5 to 0.75 which then necessarily results in lower efficiency than with ideal 1/L scaling. Additionally, we postulate that the geometrical ΔR should be modified into effective ΔR that accounts for the sheath and presheath thickness. This thickness does not contribute in generating thrust and brings the predicted i and η more in line with experimental observations. The effective ΔR is then

$$\Delta R_S = \Delta R - 2\lambda_d = \Delta R - 2k_S\sqrt{\frac{\varepsilon_o T_e}{n_e q}} \qquad [12]$$

where the reader recognizes λ as the Debye length which is of the order of the sheath thickness. The presheath can be 100 times thicker which we account for by the factor k_S that is typically selected to be 1 to 10 (i.e. up to 10% of the presheath thickness is assumed not to contribute to performance). The t_{iloss} time (Eq. [6]) then uses ΔR_S instead of ΔR such that

$$\tau_{iloss} = \frac{\Delta R - 2k_S\sqrt{\frac{\varepsilon_o T_e}{n_e q}}}{2\sqrt{\frac{qT_e}{m_i}}} \qquad [13]$$

Because the above equation contains n_e the integration of Eq. [4] should include Eq. [13]. This would however make it impossible to solve analytically and therefore we assumed that in Eq. [13], n_e can be approximated by αn_n where α is typical ionized fraction (~ 0.05).

We evaluated Eq. [7] using Eq. [13] for τ_{iloss} and typical values for the inputs while scaling *B* and n_n as $L^{-3/4}$. The predicted i and η values, versus thruster size, exhibit trends consistent with the limited available data. Figure 2 shows i and η versus "nominal" thruster discharge power for ideally scaled thruster (~1/L) and non-ideally scaled thruster ($\sim(1/L)^{0.75}$) with both scaling approaching accounting for the sheath thickness as expressed by Eqs. [12] and [13]. It is seen that the efficiency (η) for a 50 W thruster designed for achievable B and tolerable n_n (i.e. non-ideal scaling) is only 5% and i exceeds 0.9 which means that most (over 90%) of the primary charges are lost to walls.

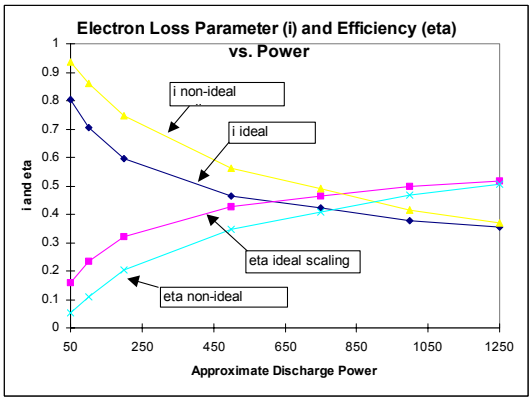

Figure 2 Electron loss parameter i and efficiency η are plotted versus a nominal thruster power for 2 different self similar scaling procedures. The ideal scaling is B and nn as (1/L), non ideal scaling which is more physically realistic is (1/L)0.75. Both the ideal and nonideal scaling includes effects of wall sheath (ksλ).

Based on the above results supported by experimental data[10,11] we conclude that operating 200 W thruster in a pulsed mode with 25% duty cycle is preferable over developing 50 W thruster for 100% duty cycle. The size of the capacitor will then have to selected such that start and shut down transients, that cause losses, are short relative to the pulse duration which is determined by the stored energy.

It is to be stressed however that the predictions in Figure 2 apply to our conventional HD style thruster[12], to SPT thrusters and to lesser extent TAL type thrusters. They do not apply to our tandem style thruster[8], which is more efficient in the low power range. Nevertheless the trend applies to all design styles including the tandem style BHT-200.

4.0 Modeling of the Electrical Transients

Modeling of the electrical transient is necessary to understand what governs the start up time which must be minimized for an effective pulsed Hall thruster. We have approached the problem from an electrical engineering point of view while incorporating enough of plasma physics to capture the essential features of the discharge.

The electrical schematic of the capacitively driven Hall thruster is shown in Figure 3. Capacitance C_S is charged to a voltage of V_S and switch S_2 is closed discharging C_S through the plasma which is represented by a resistor R_d and capacitance C_d. Under high frequency of start up transients all plasmas exhibited capacitive load features which may be important to capture because they are geometry and hence thruster dependant. The thruster electromagnet, in series with the discharge, is represented by the inductance L_m, resistance R_m and associated parasitic capacitance of the coil C_m. The inductance L_w represents the combined lumped inductance of all wiring. Ignoring the charging power supply as irrelevant when S_2 closes, the circuit is a simple R-L-C loop described in all basic texts. What makes it a unique, highly nonlinear problem is the dependence of the plasma resistance R_d on the applied magnetic field B and hence on the discharge current which in turn depends on the ionization rate and electron and neutral number densities. Therefore we first describe the approach to modeling R_d before presenting the circuit equations.

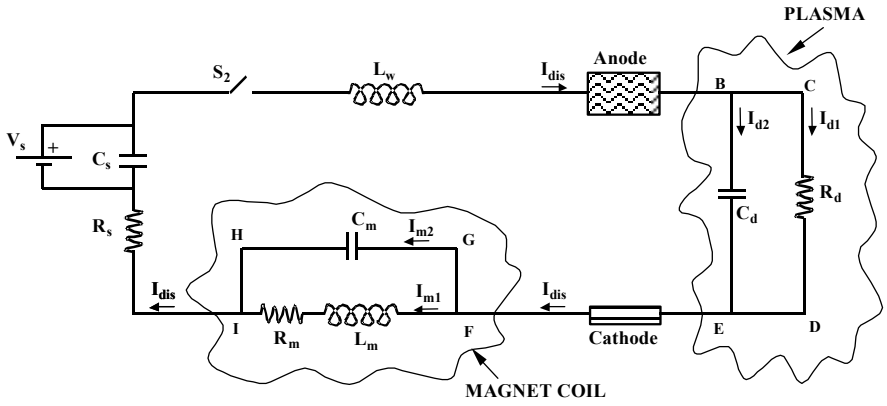

Figure 3 Electrical schematic of the capacitively driven Hall thruster

The electron axial current density (J) is given[13] by

$$J = \frac{qn_e}{16B}\frac{dV}{dx} + \frac{qT_e}{16B}\frac{dn_e}{dx} \qquad [14]$$

where q is electron charge, n_e is electron number density and dV/dx is the axial electric field. Ignoring dn_e/dx ferm leads to R_d described by the Bohm diffusion expression

$$R_d \cong \frac{V_d}{I_{d\,is}} \cong \left(\frac{\ell}{A_{exit}}\right)\frac{16B}{qn_e} = \frac{16B}{\pi d_m q n_e} \qquad [15]$$

where ℓ is the interaction length of the thruster and A_{exit} is the thruster exit area. This ratio can be approximated as πd_m where d_m is the thruster cavity

mid diameter. Amperes law is used to approximate B as

$$B \cong \frac{\mu_o I_{d\,is} N_c}{\Delta R_p} \qquad [16]$$

where N_c is the electromagnet coil(s) number of turns and ΔR_p is the radial gap between the magnetic poles. To be accurate the I_{dis} should be replaced with I_{m1}, however on the time scale of the expected B variations $I_{dis} \approx I_{m1}$. The transient magnetic field however does not obey the above equation because it requires finite amount of time to diffuse through the magnetic structure of the thruster. A fast rising I_{dis} induces opposite current in the magnetic structure (the so called eddy current) that tends to slow down the rise of the magnetic field B. To estimate the time lag between I_{dis} and B we use the skin effect equation

$$\tau_{md} = \pi\delta^2 \frac{\mu}{\rho} \qquad [17]$$

where τ_{md} is the magnetic diffusion time, δ is characteristic thickness of the magnetic structure (iron), μ and ρ are its permeability and electrical resistivity respectively. We then assume that B is exponentially dependant on τ_{md} which combined with Eq. [16] yields

$$B \cong \frac{\mu_o I_{dis} N_c}{k_1 d_m}\left(1 - e^{-t/\tau_{md}}\right) \qquad [18]$$

where ΔR_p was replaced with $k_1 d_m$. Thus at $t=0$, $B=0$ regardless of I_{dis} and when $t >> \tau_{md}$, Eq. [18] reduces to Eq. [16]. Combining Eq. [15] with Eq. [18] yields

$$R_d = k_2\left(\frac{I_{dis}}{n_e}\right)\left(1 - e^{t/\tau_{md}}\right) \qquad [19]$$

where the constant $k_2 = 16\mu_0 N_c / \pi q k_1 d_m^2$. Thus the plasma resistance at $t=0$ is zero regardless of I_{dis}/n_e. In reality R_d at $t=0$ is near infinity because the propellant breakdown is just being initiated while the I_{dis} is flowing into the capacitor C_d. Thus one way to estimate this discharge ignition time is to estimate the time to charge C_d to some breakdown voltage. For the circuit of Figure 3 τ_{ig} is:

$$\tau_{ig} = 2\left(\frac{V_{ig}}{V_s} C_d L_w\right)^{1/2} \qquad [20]$$

where V_{ig} is the experimentally observed discharge ignition voltage, typically about 50 volts or less. We then assume that R_d is also an exponential function of τ_{ig} yielding the overall expression

$$R_d = k_2 \frac{I_{dis}}{n_e}\left(1 - e^{t/\tau_{md}}\right) + R_{bi} e^{-t/\tau_{ig}} \qquad [21]$$

where R_{bi} is the large resistance of the gas before ignition (some MΩ). This expression behaves in time as we would expect, high R_d at $t=0$ decreasing to a minimum and then slowly rising as the magnetic field increases.

While one can assume some initial ($t=0$) electron number density, the n_e contained in Eq. [21] must be calculated in time. We use ionization rate equation

$$\frac{dn_e}{dt} = n_e n_n \sigma_i U_e \qquad [22]$$

where n_n is neutral atom number density, σ_I is the ionization cross-section and U_e is electron impact velocity. Most of the ionization is accomplished by the azimuthal electron drift. Thus it is reasonable to replace U_e with $E_z/B = dV/dx/B$ which we can combine with the first term in Eq. [14] to yield

$$U_e \cong \frac{I_{dis} R_d}{\ell}\frac{1}{B} \cong \frac{I_{dis}}{n_e}\frac{16}{\pi d_m \ell q} \qquad [23]$$

combining Eq. [22] and [23] yields

$$\frac{dn_e}{dt} = \frac{16 n_n \sigma_i I_{dis}}{\pi d_m \ell q} = k_3 n_n I_{dis} \qquad [24]$$

where the constant k_3 is defined by the above equation and is set by the thruster geometry. Note that non-zero dn_e/dt can be obtained even if R_d is high ($\approx R_{bi}$) because $I_d \neq 0$ flowing into the capacitor C_d. This is saying that ionization starts occurring

immediately upon closing switch S_2 as long as there is sufficient gas pressure ($\sim n_n$) and there is an operating external cathode.

The plasma capacitance was estimated by using an effective anode area, A_a and a sheath thickness Δx of the order of the Debye length.

$$C_d = \frac{\varepsilon_o A_a}{\Delta x} \qquad [25]$$

where ε_o is the permittivity of free space.

Standard circuit analysis yields a set of eight equations, for the eight unknowns I_{dis}, V_s , V_d, V_m, I_d , I_{m1}, I_{d2}, I_{m2}. These equations are:

$$\frac{dI_{dis}}{dt} = \left(\frac{1}{L_w}\right)\left(V_s - R_s I_{dis} - V_d - V_m\right);$$

$$\frac{dV_s}{dt} = \frac{-I_{dis}}{C_s};\quad \frac{dV_d}{dt} = \frac{I_{d2}}{C_d} \qquad [26]$$

$$I_{d1} = \frac{V_d}{R_d};\quad \frac{dV_m}{dt} = \frac{I_{m2}}{C_m};$$

$$\frac{dI_{m1}}{dt} = \left(\frac{1}{L_m}\right)\left(V_m - R_m I_{m1}\right) \qquad [27]$$

$$I_{d2} = I_{dis} - I_{d1};\quad I_{m2} = I_{dis} + I_{m1} \qquad [28]$$

All currents I_{dis} , I_{d1} , I_{d2} , I_{m1} , I_{m2} are equal to zero at t = 0. Because currents are zero, $V_d = 0$ and $V_m = 0$ *and* V_s at t=0 is equal to some voltage input, typically we used 250 volts.

The set of Eqs. [26]-[28] with the above initial conditions were integrated numerically with inputs shown in Table 1. The results are shown in Figure 4 and Figure 5.

Figure 4shows the very early transients of the currents in the plasma, the currents in the magnet, the resistance of the plasma and the voltages V_d across the plasma and V_m across the magnet. At t = 0, V_s = 250 Volts, $dI_{dis}/dt = V_s / L_w$ or $I_{dis} = (V_s / L_w)\, t$ for t = 0+, i.e. the discharge current rises initially linearly with time. Also, at the very beginning $I_{dis} \sim I_{d2}$ since the resistance of the plasma is very large, initially, and $I_{dis} \sim I_{m2}$ since the inductance of the magnet is very large. At the very early times the current is essentially driven by the source V_s the inductance L_w and the capacitors C_d and C_m and oscillates at a frequency $(L_w C_{eq})^{-1/2}$ where C_{eq} is an equivalent capacitance ($1/C_{eq} = 1/C_d + 1/C_m$). We observed very similar oscillations experimentally.

The current I_{dis} reaches its first maximum when $V_d + V_m \sim V_s$. Notice that, since the currents I_{dis} and I_{d2} rise linearly with time, the rise of the voltages V_d and V_m is initially proportional to t^2 ($V_d = (1/C_d)(V_s/L_w)\, t^2/2$ and similarly $V_m = (1/C_m)(V_s/L_w)\, t^2/2$ for t = 0+). Thus the voltages V_d and V_m also oscillate.

Figure 4(c) shows the resistance of the plasma (Eq. [21]), i.e. the sudden decay according to the second term in Eq. [21] followed by a slow rise according to the first term. The resistance reaches a minimum during the very early transient period. At around that time the current I_{d2} becomes very small since the current I_{d1} can now easily flow through the resistor. I_{d1} is now almost equal to I_{dis} and both I_{d1} and I_{dis} rise with time. The voltage V_d across the plasma also starts to rise since the resistance R_d of the plasma rises and consequently, the voltage V_m starts to drop.

Figure 5 shows the whole history of the starting transients in the thruster. The currents I_{dis} and $I_{d1} \sim I_{dis}$ reach a maximum value and then start to slowly decay to a steady state value as the resistance in the plasma rises with time to its steady state value. The current I_{m1} follows the same history since $I_{m1} \sim I_{dis}$. The currents I_{d2} and I_{m2} approach zero after 0.2 milliseconds.

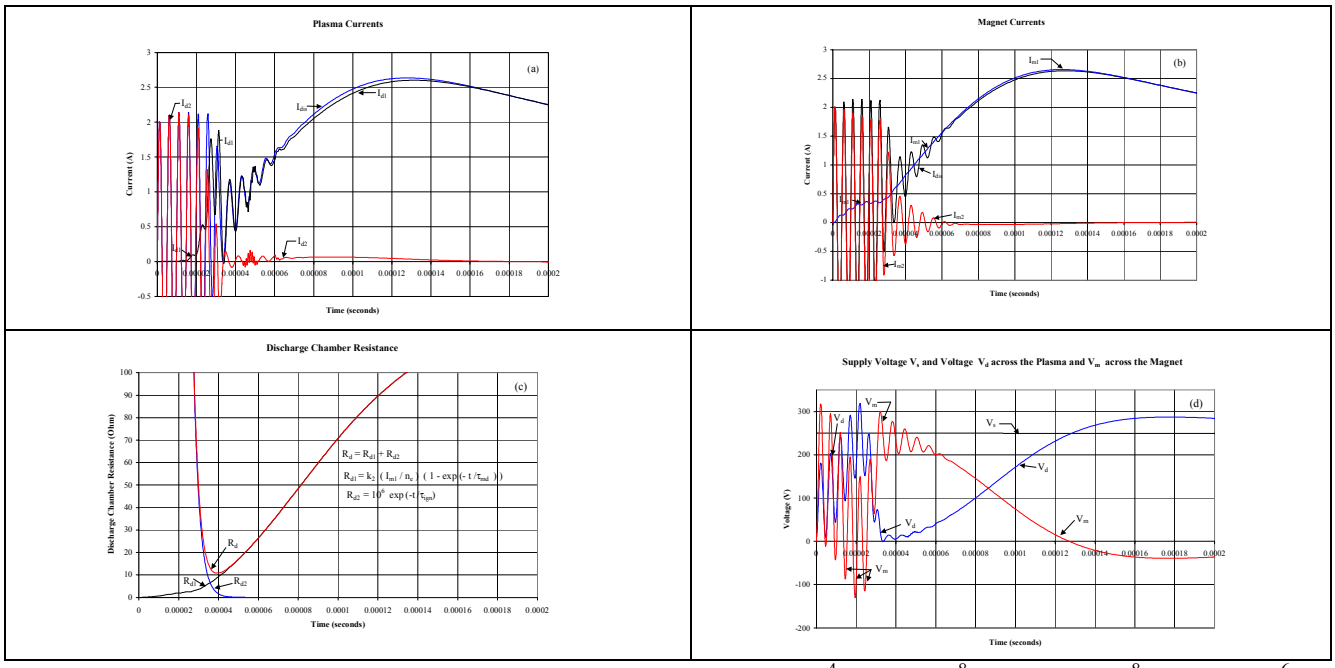

Figure 4 Early transients in the BHT-200 Hall thruster. $L_w=10^{-4}$H, $C_m=10^{-8}$F, $C_d=1.8\text{x}10^{-8}$F, $\tau_{ig}=3\text{x}10^{-6}$ sec, $\tau_{md}=2.1\text{x}10^{-2}$sec.

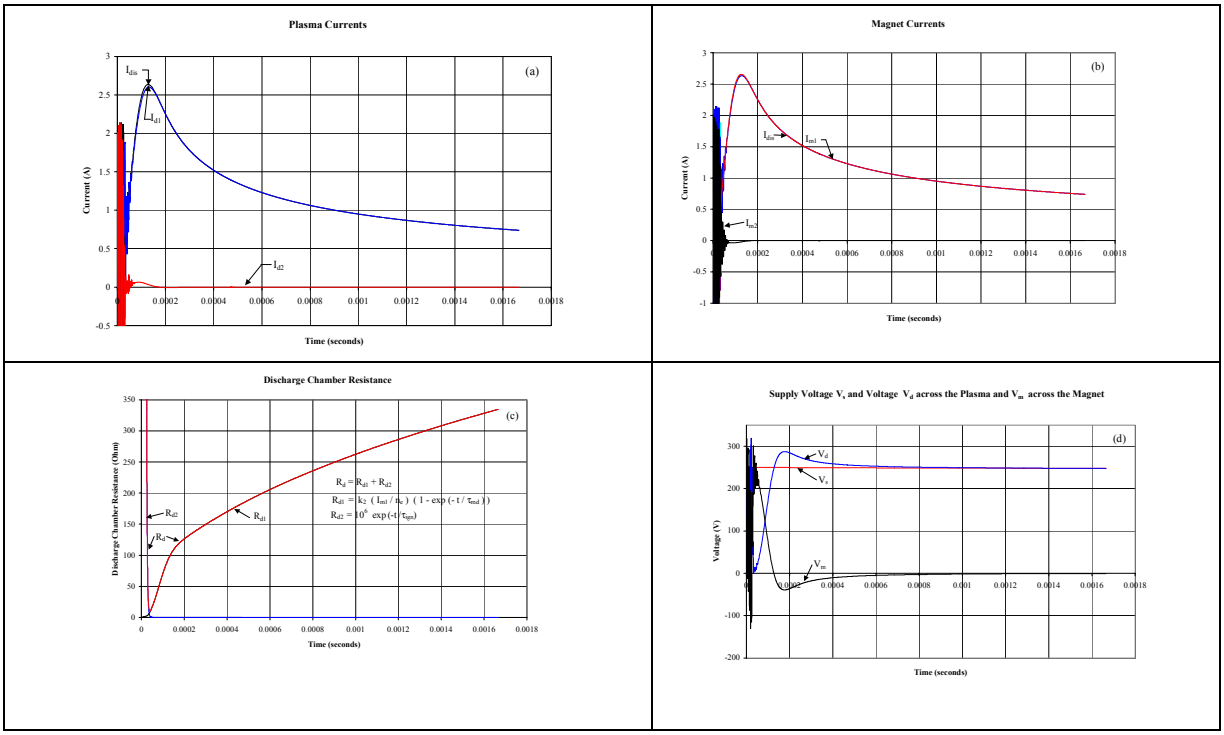

Figure 5 Start-up transients history in BHT-200 Hall thruster. Lw=10-4H, Cm=10-8F, Cd=1.8x10-8F, τig=3x10-6 sec, τmd=2.1x10-2sec+

Table 1 Input Parameters

Circuit and Magnet	
Source Capacitance	$C_s = 8.0 * 10^{-4}$ F
Magnetic Coil Parasitic Capacitance	$C_m = 1.0 * 10^{-8}$ F
Magnet Inductance	$L_m = 6.0 * 10^{-3}$ H
Inductance of wiring	$L_w = 1.0 * 10^{-4}$ H
Resistance of wiring	$R_s = 1.0\ \Omega$
Magnet Resistance	$R_m = 1.0\ \Omega$
Magnetics	
Number of Magnet Coil Turns	$N_c = 1000$
Relative/effective Permeability of Magnetic Circuit	$\mu_r = 100$
Resistivity of Iron / Magnetic Structure	$\rho = 4.0 * 10^{-7}\ \Omega$ m
Characteristic Thickness of Magnetic Structure	$\delta = 0.00462$ m
Thruster and Plasma	
Mid Diameter of Discharge cavity	$d_m = 0.08$ m
Effective Anode Area	$A_a = 0.02$ m^2
Characteristic Length of Discharge Cavity	$\ell = 0.01$ m
Constant $k_1 = d_m / \Delta R_p$	$k_1 = 0.3$
Ionization cross-section	$\sigma_i = 8.0 * 10^{-18}$ m^2
Sheath Thickness (Debye Length)	$\Delta x = 0.00001$ m
Plasma Ignition Voltage	$V_{ig} = 50$ V
Plasma Resistance before Ignition	$R_{bi} = 1.0 * 10^6\ \Omega$
Electron Number Density	$n_e = 3.5 * 10^{15}$
Neutral density	$n_n = 1.0 * 10^{18}$

The predicted behavior of the discharge current (I_{dis}) shown in Figure 4(a) and Figure 5(a) qualitatively agrees with the measured values shown in Figure 6. The measured peak value is $I_{dis} \approx$ 3.2 Amps (excluding the high frequency peaks) which occurs about 0.2 msec after start. The predicted I_{dis} reaches 2.6 Amps in 0.12 msec. The predicted very high frequency noise in the first 0.04 msec is also discernable in the measured trace.

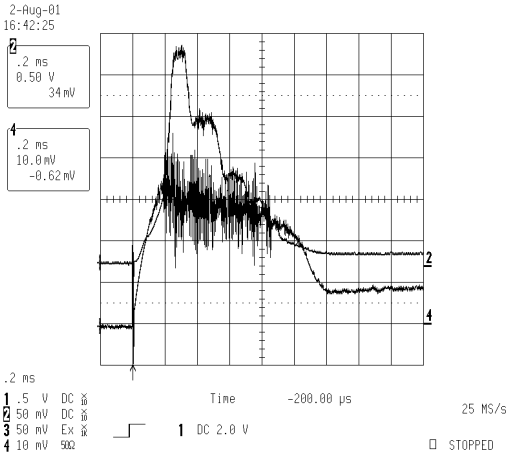

Figure 6 Measured discharge current (lower trace) using 0.8 mF capacitor and magnetic coil in series with the discharge. The upper trace is UV light output from the discharge indicating that most of the

initial discharge energy, when magnetic field is near zero, is converted to light.

Of significant interest is the diffusion time of the magnetic field which we modeled by the skin effect (Eqs. [17] and [18]). To confirm our approach we measured the B-field in the gap of the BHT-200 placed on a bench top. The measured coil voltage current and flux density (B) are shown in Figure 7. The current was driven by a power supply which determines the rate of rise of the voltage and the current that is much slower than that achieved by capacitor discharge. The power supply was current limited to 1.5 Amps. Of importance in this figure is the fact that B increases long after the current is constant giving clear demonstration of induced eddy currents in the magnetic structure that oppose generation of B. When the eddies die out, B reaches steady state as predicted by Eq. [18].

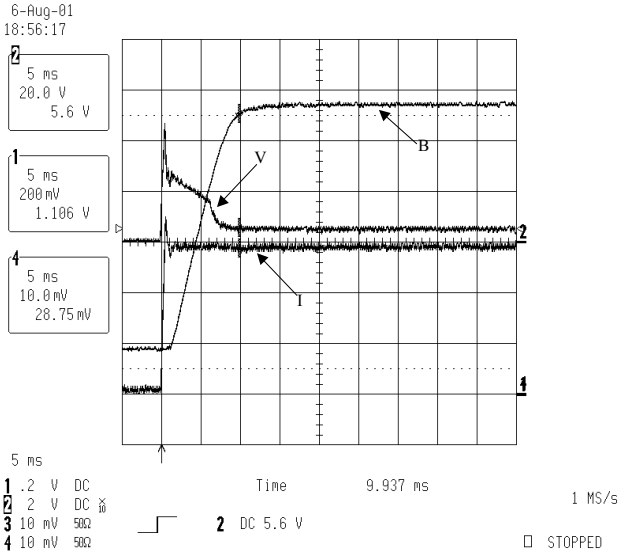

Figure 7 Measured thruster magnet coil voltage (V), current (I) and gap flux density (B) with the thruster on a bench Isp. The power supply was current limited to 1.5 A. The B increases about 6 msec after I reached steady state and required a total of 10 msec to reach a DC level. The predicted $\tau_{md} \approx 20$ msec.

5.0 Modeling of the Flow Transients

To achieve high average Isp with a pulsed thruster, approaching that of steady state operation, the flow ramp up and down should be as steep as possible. To determine what governs the starting range and to understand better our data we constructed a simple model described below.

The difference between the flow into the discharge chamber ($\dot{m}_{in}$) and the flow exiting the discharge chamber ($\dot{m}_{out}$) is equal to the propellant build up within it

$$\dot{m}_{in} - \dot{m}_{out} = V_c \dot{n} m \qquad [29]$$

where V_c is the discharge cavity volume, $\dot{n}$ is the rate of change of neutral number density within V_c and m is the atomic mass of the propellant.

The exiting flow (before application of power) can be approximated by

$$\dot{m}_{out} = cnA_{exit}m \qquad [30]$$

where c is the propellant speed of sound and A_{exit} is the discharge chamber exit area.

Assuming that the propellant injectors are chocked, the injected mass flow is

$$\dot{m}_{in} = \frac{p_m A_{in}}{\sqrt{T_0}} \sqrt{\frac{\gamma M}{R}\left(\frac{2}{\gamma+1}\right)^{(\gamma+1)/(\gamma-1)}} = k_1 p_m \qquad [31]$$

where p_m is the propellant pressure in the manifold, T_o is the propellant stagnation temperature assumed to be equal to static T, γ is the ratio of specific heats of the propellant, M is its mass/mole and R is the universal gas constant. All these variables with the exception of p_m are treated as invariant with time. To estimate the pressure build up within the manifold when the propellant valve instantaneously opens, we assumed that the pressure upstream of the valve is constant (p_o) and used 1D momentum equation

$$\rho u \frac{du}{dx} = \frac{dp}{dx} \qquad [32]$$

where ρ is the propellant density and u its flow velocity from the valve into the manifold. Replacing

ρ with p using equation of state while assuming that T = constant allows simple integration of Eq. [32] and yields

$$p = c_1 \exp\left[-\left(\frac{Mu^2}{2RT}\right)\right] + c_2 \qquad [33]$$

where c_1 and c_2 are constants of integration. Approximating u as

$$u \cong \frac{V_{mt}}{A_t t} \qquad [34]$$

where V_{mt} is the volume between the valve and the injectors and includes the manifold and the tubin, A_t is the tubing flow area and t is time. The valve opens instantaneously at t=0 when the manifold is empty with internal pressure equal to the tank pressure (p_t). At t = ∞ the manifold pressure must be equal to the constant pressure upstream of the valve (p_o). Substituting Eq. [34] into Eq. [33] and applying the above conditions to evaluate c_1 and c_2 yields

$$p_m = (p_o - p_t)\exp\left[-\frac{M}{2RT}\left(\frac{V_{mt}}{tA_t}\right)^2\right] + p_t \qquad [35]$$

Substituting Eqs. [35], [31] and [30] into Eq. [29] yields a first order non-linear differential equation

$$\frac{dn}{dt} + \frac{n}{\tau_{cf}} = \frac{k_1 p_t}{V_c m} + \frac{k_1 (p_o - p_t)}{V_c m}\exp\left[-\left(\frac{\tau_{mf}}{t}\right)^2\right] \qquad [36]$$

where k_1 is a constant defined by Eq. [31] and the characteristic times for the discharge chamber and manifold filling are τ_{cf} and τ_{mf} respectively. They are defined as

$$\tau_{cf} = \frac{V_c}{A_{exit}}\sqrt{\frac{M}{\gamma RT}} \qquad [37]$$

$$\tau_{mf} = \frac{V_{mt}}{A_z}\sqrt{\frac{m}{2RT}} \qquad [38]$$

Using the BHT-200 dimensions for calculating V_c, V_{mt}, A_{exit}, A_t and T = 300°K, γ = 1.66, M = 131 kg/kmole and m = 2.17E-25 kg, yields $\tau_{cf} \cong$ 0.4 msec and $\tau_{mf} \cong$ 3 msec

Equation [36] was integrated numerically with t=0 number density given by n = p_t/kT where k is the Boltzmann constant. The results are shown in Figure 8 where the non-dimensional mass flow $\dot{m}_{in}(t)/\dot{m}_{in}(t=\infty)$ is plotted versus time after opening the valve. The lower curve corresponds to the combined manifold and tube volume of V_{mt} = 4.71 cm^3 for the existing BHT-200 experimental set up. Within this present geometry the flow reaches 90% of its steady state value in about 10 msec. The experimental data indicates discharge turn on in about 15 msec. We attribute longer time to delays in valve operation and perhaps lower p_o than used in the calculations because we are unsure about the propellant pressure drop in the thrust stand tubing.

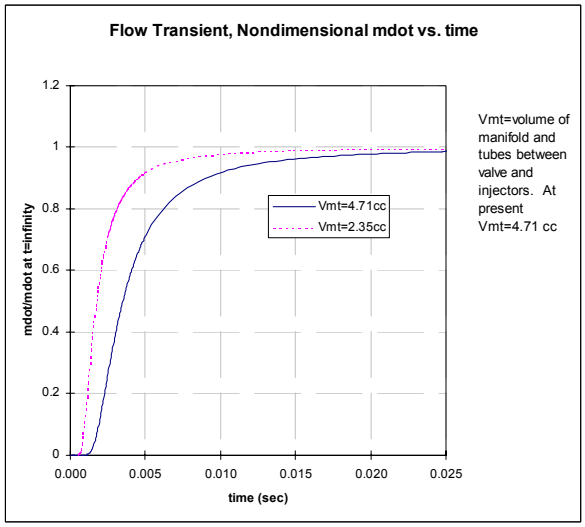

Figure 8 Predicted nondimensional thruster mass flow $[\dot{m}_{in}(t)/\dot{m}_{in}(t=\infty)]$ is plotted versus time after the propellant valve opens. The solid line corresponds to the present set up (Vmt = 4.71 cm3). The dashed line indicates that reducing Vmt by 50% reduces the filling time by about the same fraction.

Reducing V_{mt} by 50%-reduces the predicted time to reach 90% of steady state mass flow to less than 4.5 msec. Reduction of V_{mt} to optimize the thruster for pulsing is a key requirement for successful pulsed Hall thrusters. Reduced V_{mt} also facilitates shorter

time to "drain" the manifold and increase propellant utilization during the turn off transient. As seen in the previous section the measured and predicted magnetic diffusion time are 10 to 20 msec and hence comparable to the flow transient of 10 msec.

Finally it should be noted that one of the key parameter V_c/A_{exit} corresponds to the discharge cavity length and hence roughly thruster power. Therefore the flow transients, or the time to reach steady state will grow with thruster power unless specialized pulsed Hall thruster designs are evolved.

6.0 Pulsed Hall Thruster Experiments

The BHT-200 tandem style thruster[8] and the 1/8-in diameter BHC-1500 hollow cathode were used for the experiments (see Figure 9) carried out in the Busek T6 facility. The initial pulsed Hall thruster experiments were motivated by the TechSat 21 impulse requirement of 2 mNsec. These were performed by both flow pulsing and power pulsing and synchronized flow and power pulsing using conventional laboratory power supplies connected to the thruster via a high voltage fast acting switch. Subsequent experiments were carried out with capacitive drive synchronized with flow pulsing.

During most the experiments the cathode was either preheated or operating on the keeper. Some later experiments were carried out with TechSat 21 PPU breadboard which contains all the converters (discharge, magnet, cathode heater, cathode keeper and starter) controlled by PC via a LabView software. Over the course of the experimental program nearly 500,000 pulses of various duration were accumulated without detecting any problem with either the thruster or the cathode. A large set of data was collected and below we present selected samples.

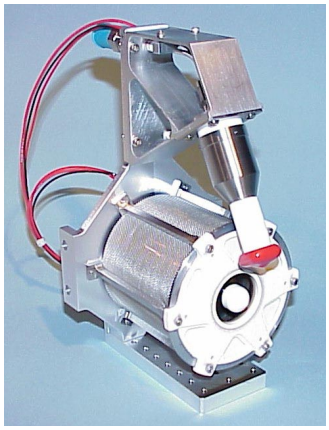

Figure 9 Photograph of the typical experimental hardware BHT-200 thruster and BHC-1500 hollow cathode. Not shown is the cathode flow isolator, essential for pulsing experiments.

6.1 Power Pulsing Using Switched Power Supply

An experimental study of "power pulsing" mode is shown in Figure 10 through 15. Representative discharge current and voltage pulses are shown in Figure 10 and Figure 11 illustrating a subsecond pulse and about a 3 second pulse, respectively. It is evident that the time to transit from zero to near steady state discharge voltage and discharge current is very short relative to the pulse length. The oscillatory response of a thrust stand to the thruster pulse was integrated form 0^- to "near infinity" and the results for typical pulses with varying duration are shown in Figure 12 and Figure 13. The data show that any impulse from a sub mN sec and up can be obtained and that the existing invested pendulum NASA GRC type thrust stand can record it.

The average thrust for varying pulse length is plotted in Figure 14, for two different discharge voltages. To assess the thruster performance in pulsed mode relative to steady state – continuous operation mode, the average pulsed thrust in Figure 14 was non-dimensionalized by a steady state thrust measured at same mass flow and discharge voltage. This non-dimensionalized thrust is shown in Figure 15, documenting that the pulsed thrust is very nearly equal to the steady state thrust, for pulses with duration of the order of 0.1 sec or longer.

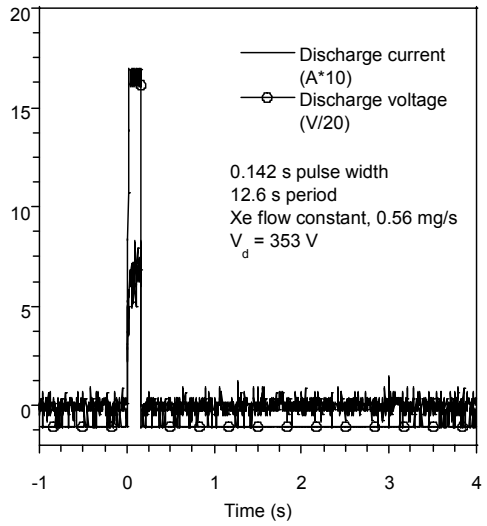

Figure 10 Discharge voltage and current versus time. 0.142 s pulse width

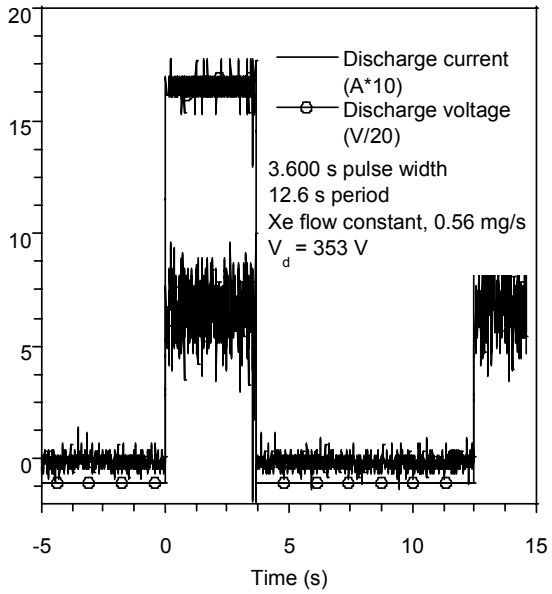

Figure 11 Discharge voltage and current versus time. 3.600 s pulse width

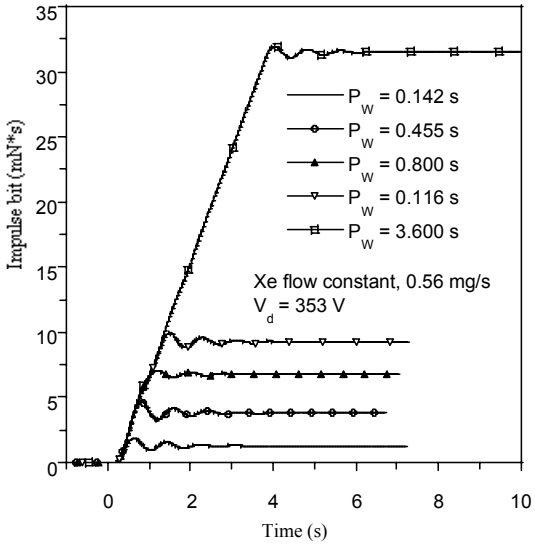

Figure 12 Time integral of balance output for different pulse width

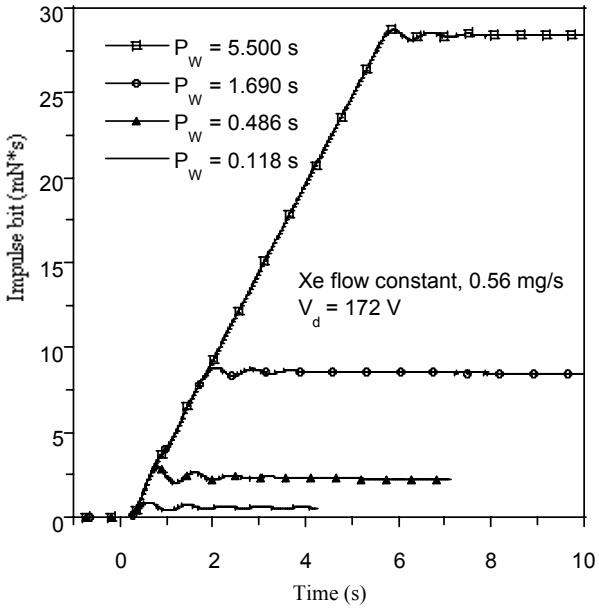

Figure 13 Time integral of balance output for different pulse widths. VD = 172 V

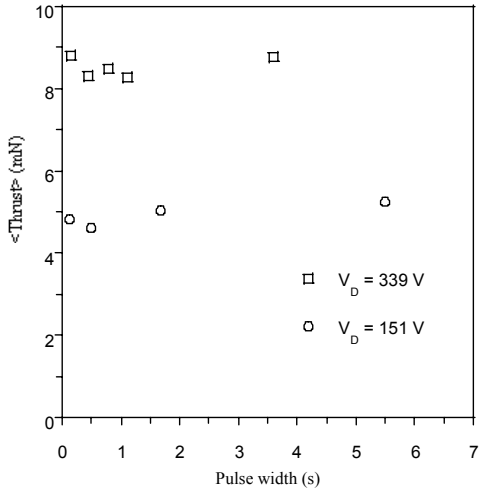

Figure 14 Average Thrust, $\langle T \rangle = \frac{1}{Pw}\oint_o^{Pw} T dt$ versus pulse width

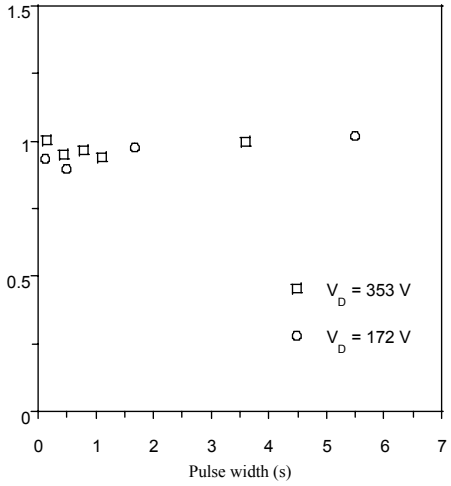

Figure 15 Ratio of average thrust, $\langle T \rangle = \frac{1}{Pw}\oint_o^{Pw} T dt$ to steady state thrust versus pulse width

6.2 Power Pulsing Using Capacitive Drive

Representative data from capacitvely driven thruster (See Figure 1) with steady state continues flow are shown in Figure 16 and Figure 17 a, b, c. The discharge period was fixed at 50 msec. The thruster and cathode Xe mass flows were 0.94 and 0.08 mg/sec respectively. A 0.8 mF capacitor bank was charged to 250 Volts and dropped down to 200 Volts during the discharge period. The average discharge power was approximately 180 watts drawing 9 joules of energy from the capacitors.

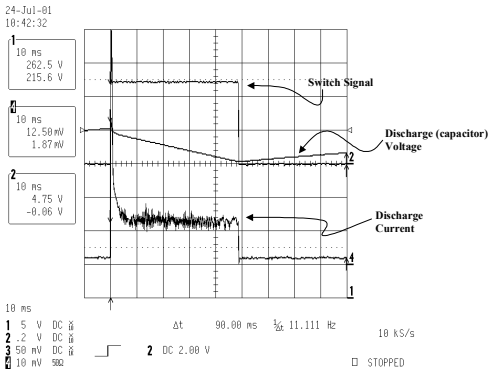

Figure 16 Typical oscilloscope traces for a 50 msec discharge pulse at the nominal steady state thruster mass flow rate.

An oscilloscope trace typical of the discharge characteristics is shown in Figure 16. Trace 1 shows the discharge voltage, Trace 2 is the 5 V trigger input to the power switch and Trace 4 is the discharge current. When the switch closes we typically see an initial spike in the discharge current that drops to the steady state current in less than 10 msec. The typical spike reaches 3 to 4 amps are about 3 to 4 times DC value. High frequency oscillations occur in the first 0.5 to 1 msec when most of the input energy is converted to light (see Figure 6). All this data is consistent with predictions presented in earlier sections. When the switch opens the discharge current goes to zero and the charging power begins re-charging the capacitors to the starting voltage of 250 V. This is seen by the positive slope of the discharge voltage trace. Figure 17 shows oscilloscope traces of multiple 50 msec discharge pulses when the charging power is varied from 10-50 W. As the charging power increases the charging time is reduced accordingly. As we would expect the charging time has no impact on the discharge characteristics.

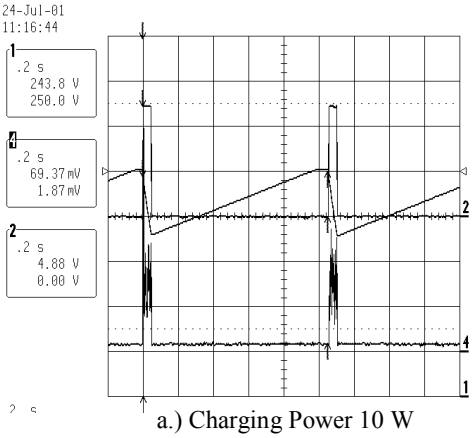

a.) Charging Power 10 W

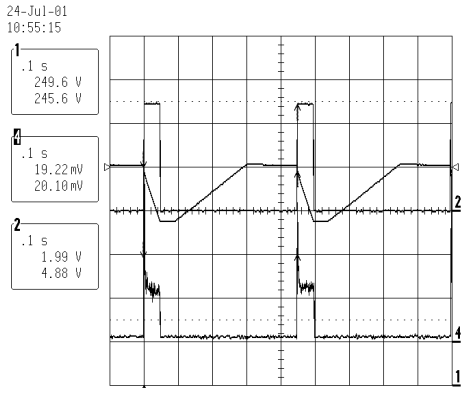

b.) Charging Power 25W

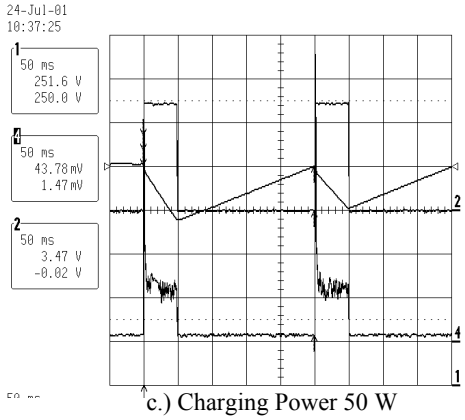

c.) Charging Power 50 W

Figure 17 Multiple 50 msec discharge pulses for 10, 25 and 50 W of charging power.

Comparing the measured impulse bit during pulsed operation to the theoretical performance we obtain about 85% of the DC/steady state performance. This corresponds to an effective anode thrust efficiency of about 40% during a 50 msec pulse. For a pulse width of 25 msec the percentage drops to about 70%. This is caused by the starting transient occupying a larger fraction of the total pulse duration. With a steady flow input the only significant transient is the magnetic diffusion time which was analytically estimated to be as long as 20 msec (see Eq. [17]) and measured between 5 to 10 msec depending on the magnet driving voltage.

To achieve an average Isp comparable to the steady state Isp (>1000 sec), the flow must pulsed at the same frequency as the power. A fast acting valve installed just upstream of the thruster was used for this purpose (see Figure 1). The duration of the valve opened period and the off set with respect to the power pulse were varied. Representative results are plotted in Figure 18 which shows the actual thrust and I_{sp} during a 50 msec pulse while the delay time between the flow valve trigger signal and closing the discharge switch was increased from zero to 80 msec. We see the thrust peaks at a delay time of 30-40 msec corresponding to the time required for the neutral density to reach steady state. This is longer than was estimated using the analytical model described earlier by about a factor of 2 to 3. Uncertainties in the pressure drop inside the thrust propellant tubing and the valve are the likely cause for the discrepancy.

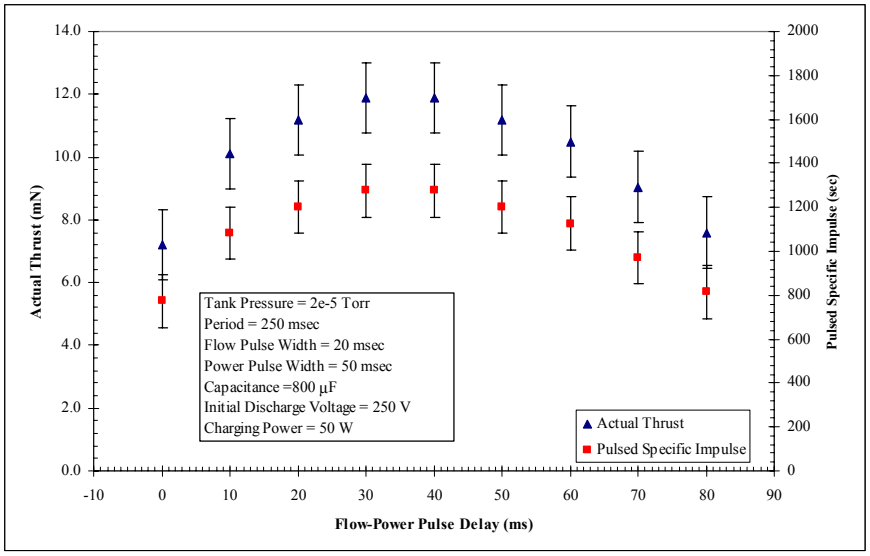

Figure 18 Thrust and Isp for a 50 msec discharge pulse. Performance peaks at a 30-40 msec delay between the flow and power trigger signals.

7.0 Discussion

The experiments and analysis clearly demonstrated that pulsing the BHT-200 thruster is feasible and an excellent method to achieve nearly arbitrary impulse level and average power consumption. The magnetic diffusion time and the time to fill and drain discharge chamber are the dominant transients that determine the minimum practical discharge pulse width. To reach at least 80% of the steady state performance (thrust and Isp), the minimum pulse time is approximately 30 to 50 msec. To achieve shorter pulse time and to design any thruster for efficient pulsed operation requires the following approach

1. Reduce thruster discharge cavity volume to achieve rapid build up of neutral number density. Minimize volume between propellant valve and thruster injectors including the manifold volume. This will reduce τ_{mf} and τ_{cf}.
2. Use magnetic material with (a) lower permeability or a material with high squareness ratio (i.e. square shaped hysteresis curve); (b) high electrical resistivity; (c) laminated or segmented magnetic structure; (d) consider the use of small permanent magnets. Employing any or all of these steps will reduce τ_{md} (reduce eddy currents) and increase the rate of rise of magnetic field. Alternatively use a separate or a switched power source (capacitor) to start the coil current some msec before the discharge starts.
3. Use magnet coil winding techniques that minimize parasitic coil capacitance and avoid conductive bobbins especially if the discharge is in series with the coil.
4. Reduce thruster plasma capacitance which means reduce thruster anode area. This will reduce τ_{ig}.
5. Minimize inductances in all wiring because rapid discharge current rise will induce high voltages requiring improved propellant line isolators on both the anode and the cathode.

Not included in this list, but implicit in the models, is the obvious need for rapidly starting cathode, with the heaterless and/or field emission cathodes as the first candidates.

We have evaluated two different concepts of heaterless cathode and demonstrated rapid turn on with one of them. However, it should be realized that for average discharge power consumption exceeding 50 watts, the existing 1/8-in. hollow cathode (BHC-1500) does not have unacceptable impact on the system Isp and efficiency. A continuous keeper power of the order 10 watts and

flow of 0.05 mg/sec is sufficient for instantaneous turn on at 4 Hz rep rate.

A mission that requires significant total impulse may require a fast acting valve capable of 10^7 cycles. Flight qualified valves with 10^6 cycles exist[14], commercial (not space qualified) valves with 10^8 cycles exist[15] and redundant MEMS type valves are in development[16].

Detailed description of the capacitive drive experiments and results along with a description of the heaterless cathode and the complete PPU breadboard controlled by LabView software which was used in some of the pulsed experiments is planned for future publications.

8.0 Conclusions

The feasibility of low power pulsed Hall thruster operation was demonstrated. Pulsed 200 W thruster appears preferable over, for example, 50 W thruster operating continuously. Electrical and fluid dynamic analytical models of the pulsed Hall thruster starting transients were constructed. The predicted magnetic diffusion and flow starting transients are comparable, of the order of 10-20 msec. These can be expected to grow linearly with thruster size/power.

During the test program we have accumulated nearly 0.5 M pulses with no evidence of any degradation. At 50 msec pulse duration, the unoptimized capacitively driven system delivers approximately 80% of the steady state thrust and Isp. This performance level makes the pulsed low power Hall thruster competitive against other low power EP devices such as micro ion engines, large FEEPs and colloids and most importantly the PPTs. The PPT's major advantage is lower system complexity which the pulsed Hall can counter by a heaterless cathode and simplified PPU with the ultimate solution being direct capacitor charging from the spacecraft bus – the so call direct drive. The pulsed Hall can deliver precisely tailored impulse bits starting from sub mNsec to 10^5 Nsec for PPU driven systems. In principal the pulsed Hall thruster can operate at any average discharge power. For present system the practical limit is approximately 10 Watts with a unoptimized pulse duration greater than 30 msec. The parameters that govern pulsed operation of any thruster include the magnetic diffusion time caused by eddy currents and by the flow on/off transients. Design approaches to reduce both the electromagnetic and the fluid dynamic transient were identified.

Acknowledgements

The presented material is the result of an internally funded effort and two government sponsored programs including the (1) TechSat21 propulsion program sponsored by AFRL lead by Mr. Daron Bromaghim and (2) NASA GRC Phase I SBIR program entitled "Xenon Fueled Electric Micro-Thruster" lead by Mr. Robert Jankovsky. The authors thank AFRL and NASA for the opportunity to work on this exciting technology.

1 Hrbud, I., et al., "TAL Performance and Mission Analysis in a CDL Capacitor Powered Direct-Drive Configuration," 33rd Joint Propulsion Conference, Seattle, WA, July 1997.

2 Oleson, S., et al., "Sample Mission Application of Capacitor Powered Hall Thrusters," 33rd Joint Propulsion Conference, Seattle, WA, July 1997.

3 Christensen, Jon A., et al., "Design and Fabrication of a Flight Model 2.3 kW Ion Thruster for the Deep Space 1 Mission," AIAA 98-3327, *34th AIAA/ASME/SAE/ASEE Joint Propulsion Conference*, Cleveland, OH, July 1998.

4. Chojnacki, K. and Reinicke, R., "Xenon Resistojet Design and Development," IEPC 99-022, 26th International Electric Propulsion Conference, Kitakyushu, Japan, October 1999.

5 Spanjers, G., AIP Conference Proceedings, Vol 387, Issue 1, pp. 323-328, January 1997.

6 Schilling, John H., et al., "Micropropulsion Options for the TechSat21 Space-Based Radar Flight," **Micropropulsion for Small Spacecraft**, Micci, Michael M., Vol. 187.

7. Chen Z. and Brandhorst H., "Performance of High Power Capacitors for Pulsed Plasma Thruster Applications", IEPC 99-060, 26th International Electric Propulsion Conference, Kitakyushu, Japan, October 1999.),

8 Tandem Thruster Patent, U.S. Patent No. 6,150,764, Dated Nov. 21, 2000

9 Hruby, V., et al., "Development of Low Power Hall Thrusters," 30th Plasmadynamics and Lasers Conference, Norfolk, VA, July 1999.

10 Khayms, V., Martinez-Sanchez, M., "Fifty-Watt Hall Thruster for Microsatellites," **Micropropulsion for Small Spacecraft**, Micci, Michael M., Vol. 187.

11 Arkhipov, B., et al., "Study of Stationary Plasma Thruster of Power 150…350 W," IEPC-99-095, 26th International

Electric Propulsion Conference, Kitakyushu, Japan, October 1999.
12. Hall Field Plasma Accelerator with an Inner and Outer Anode Patent, U.S. Patent No. 6,075,321, Dated June 13, 2000
13 Kaufman, H.R., "Theory of Ion Acceleration with Closed Electron Drift,", AIAA-82-1919, *16th IEPC,* New Orleans, LA, November 1982
14 Moog Space Products Division, Xenon Solenoid Valve Model # 51E186 and #51E190
15 Lee Company, LIF serried Solenoid Valve, Configuration A, $2x10^9$ cycles with clean air, 200 M cycles warrantied.
16 Cardin, J. and Otsap, B., "A Digital Xenon Flow Controller Based on ChEMS™ Technology," AIAA-99-2563, 35th AIAA/ASME/SAE/ASEE Joint Propulsion Conference, Los Angeles, CA, June 1999.